Concentric-ring structures in an atmospheric pressure helium dielectric barrier discharge*

Shang Wan-Li(尚万里)[a)†], Zhang Yuan-Tao(张远涛)[b)], Wang De-Zhen(王德真)[c)], Sang Chao-Feng(桑超峰)[c)], Jiang Shao-En(江少恩)[a)], Yang Jia-Min(杨家敏)[a)], Liu Shen-Ye(刘慎业)[a)], and M. G. Kong[d)]

[a)] *Research Center of Laser Fusion, China Academy of Engineering Physics, Mianyang* 621900, *China*
[b)] *School of Electrical Engineering, Shandong University, Jinan* 250061, *China*
[c)] *State Key Laboratory for Materials Modification by Laser, Ion and Electron Beams, School of Physics and Optoelectronic Technology, Dalian University of Technology, Dalian* 116024, *China*
[d)] *Department of Electronic and Electrical Engineering, Loughborough University, Leicestershire LE11 3TU, UK*

(Received 12 June 2010; revised manuscript received 10 July 2010)

This paper performs a numerical simulation of concentric-ring discharge structures within the scope of a two-dimensional diffusion–drift model at atmospheric pressure between two parallel circular electrodes covered with thin dielectric layers. With a relative high frequency the discharge structures present different appearances of ring structures within different radii in time due to the evolvement of the filaments. The spontaneous electron density distributions help understanding the formation and development of self-organized discharge structures. During a cycle the electron avalanches are triggered by the electric field strengthened by the feeding voltage and the residual charged particles on the barrier surface deposited in the previous discharges. The accumulation of charges is shown to play a dominant role in the generation and annihilation of the discharge structures. Besides, the rings split and unify to bring and annihilate rings which form a new discharge structure.

Keywords: dielectric barrier discharge, plasma simulation, gas discharge
PACS: 52.25.Mq, 52.30.Es, 51.50.+v **DOI:** 10.1088/1674-1056/20/1/015201

1. Introduction

High-pressure dielectric barrier discharges (DBD) exhibit a rich variety of spatial characteristics, which reveal their underlying physics and indicate their application performance. Depending on their operating parameters and their interaction with surrounding boundaries including the electrodes, DBD may appear to be filamentary, spatially diffuse, or self-organized.[1−3] Recently, various interesting discharges under the laboratory conditions have been the subject of great interest.[4−8] For example, a concentric-ring pattern in a short-gap planar DBD is observed at a gas pressure of several hPa.[4] Spiral patterns and spiral defect chaos are also found in DBD in atmospheric argon-air mixture.[9] Similar complex patterns are reported in a needle-plane electrode configuration in atmospheric helium or atmospheric argon.[10] At a high frequency of 500 kHz, using MgO coated dielectric barriers, we find that self-organization of discharge filaments occurs with a symmetric appearance.[11] Self-organization in gas discharges may occur as unstructured and localized patterns, often known as traveling spots[12,13] or as a static striate pattern formed along the length of the discharge plasma.[14] In the time domain, these spatial discharge structures may appear periodically or chaotically.[15,16]

Complex spatial patterns in DBD are scientifically both interesting and important as their understanding is critical to the development of their diagnostics methodologies and their industrial applications.[17] At present, theoretical studies of plasma patterns in high-pressure DBD are far behind their experimental studies. This is compliant by the very few two-dimensional (2D) simulations of high-pressure DBD that are critical for theoretical studies of plasma patterns. In this paper, a self-consistent fluid model of atmospheric DBD is used to study the generation and evolution of the concentric-ring discharge structures, similar to those observed experimentally.[4,9,10] The numerical simulation in our work may provide a significant insight into the underlying physical process of the formation of concentric-

*Project supported by the National Natural Science Foundation of China (Grant Nos. 50537020 and 50528707).
†Corresponding author. E-mail: wanlishang@gmail.com
© 2011 Chinese Physical Society and IOP Publishing Ltd

ring patterns. The instability of the spontaneous filaments of a DBD plasma is simulated.[18] With spectral resolved photonic secondary processes, a fluid model for barrier discharges in air at atmospheric pressure is preformed with general finite-element software to show the movement of a filament.[19] The current patterns in physics system due to electrical current flow have been described for a certain class of systems, including certain semiconductor and gas discharge systems, by a two-layer model in terms of the electrical current density and the electrical potential.[20] In our model, the temporal and spatial evolvement of the discharge rings which form the discharge structures are analysed by the charges deposited on the barrier surface and the field in the gas gap. It should be pointed out that the discharge structures are likely to be uniform radially with a not too high frequency.[18,21,22] Recently a very interesting concentric-ring discharge structure is described by Stollenwerk,[23] and the simulations are performed in 3D and without simplifications suggested in Refs. [24] and [25]. As the frequency increases, the discharge structures become non-uniform radially. In order to investigate the discharge mechanisms with relative high frequencies, the driving frequency of the applied sinusoidal voltage is set to 100 kHz.

2. Model

We consider a typical DBD configuration, in which two thin dielectric layers are used to cover two parallel electrodes, and the dielectrically insulated electrodes are separated by a thin gas gap. In order to decrease the calculation time a simple model is used with three species, namely, electrons e, helium ions He^+ and background helium atoms He. The model includes the reactions of direct electron impact ionization and dissociated ion–electron recombination. The elementary processes and the corresponding coefficients in the model are the same as those used in Ref. [22]. The simulation of the discharge is based on the 2D continuity equations for electrons and ions, with a much simpler current conservation law to replace the Poisson equation for electric field so that the solution would automatically obey the Poisson equation.[24,25] Azimuthal symmetry is assumed and cylindrical coordinates (r–z) are used. The basic equations are:

$$\frac{\partial n_{\mathrm{e,i}}}{\partial t} + \frac{1}{r}\frac{\partial (r j_{\mathrm{re,i}})}{\partial r} + \frac{\partial j_{\mathrm{ze,i}}}{\partial z} = S_{\mathrm{e,i}}, \tag{1}$$

$$\frac{\partial E_r}{\partial t} + \frac{e}{\varepsilon_0} j_{\mathrm{c}r} = 0, \tag{2}$$

$$\frac{\partial E_z}{\partial t} + \frac{e}{\varepsilon_0} j_{\mathrm{c}z} = \frac{e}{\varepsilon_0} j_{0z}, \tag{3}$$

$$\frac{e}{\varepsilon_0} j_{0z} d = -\frac{\partial V}{\partial t} + \frac{e}{\varepsilon_0}\int_0^d (j_{z\mathrm{i}} - j_{z\mathrm{e}})\mathrm{d}z, \tag{4}$$

$$S_{\mathrm{e,i}} = Ap\mu_{\mathrm{e}} E n_{\mathrm{e}} \mathrm{e}^{-B\sqrt{p/|E|}} - \beta n_{\mathrm{e}} n_{\mathrm{i}}, \tag{5}$$

where n and j are the density and flow density of species respectively, S is the source term including generation and loss of particles, the subscripts e and i donate the electrons and ions respectively, E_{r} and E_z are the transverse and longitudinal components of the electric field respectively, j_{c} is the conductivity current density, j_0 is the total current density, ε_0 is the permittivity of vacuum. A and B are constants related with the working gas (4.4 and 14.0 respectively in helium according to Ref.[26]), p is the gas pressure and β is the recombination coefficient. In our calculation, the Schartetter–Gummel scheme is used.[24,25] The particle fluxes are as follows:

$$j_{r\mathrm{e,i}} = \mp\mu_{\mathrm{e,i}} E_r n_{\mathrm{e,i}} - D_{\mathrm{e,i}}\frac{\partial n_{\mathrm{e,i}}}{\partial r}, \tag{6}$$

$$j_{z\mathrm{e,i}} = \mp\mu_{\mathrm{e,i}} E_z n_{\mathrm{e,i}} - D_{\mathrm{e,i}}\frac{\partial n_{\mathrm{e,i}}}{\partial z}, \tag{7}$$

where D is the diffusion coefficient and μ is the mobility. The applied voltage is assumed to be

$$V = V_0 \sin(\omega t). \tag{8}$$

The secondary electron emission effect at the cathode surface is described as

$$j_{\mathrm{e}} = -\gamma j_{\mathrm{i}}, \tag{9}$$

where γ is the secondary emission coefficient and is set to 0.01. The calculation begins with a spatially uniform density for ions and electrons (both set as 10^7 cm^{-3}), and with a homogeneous electric field of 10 V/cm. The surface charge and the total discharge current density are set as zero. Electron and ion diffusion coefficients and mobilities are supposed to be constants (D_{e} = 729.4 cm^2/s, D_{i} = 0.53947 cm^2/s, μ_{e} = 486.3 cm^2/(V·s) and μ_{i} = 10.4 cm^2/(V·s)), which come from Refs. [25] and [26].

3. Results

In our numerical simulation, the background gas is helium at atmospheric pressure. The gas gap between the two dielectric plates is 2.2 mm and the thickness of each dielectric barrier is 1 mm with a permittivity of 7.5. The electrodes are assumed to be

circular with a diameter of 12 mm. The excitation frequency is fixed at 100 kHz, and the peak applied voltage is 1.6 kV. Figure 1 shows the waveforms of the applied voltage and the discharge current. The one current pulse every half cycle of the applied voltage is typical of atmospheric DBD, as observed both experimentally[10] and numerically.[22] While previous 1D simulations usually assume a transverse uniformity, our 2D simulation shows a concentric pattern. As shown in Fig. 2 for four different instants marked near the current peak in Fig. 1, the discharge current density is clearly non-uniform in the radial direction. The radially concentric-ring pattern of the current density is likely to be a result of the transverse diffusion of the background gas. As the discharge current evolves through its positive peak in Fig. 1 at the four instants of 140.6, 140.8, 141.0 and 141.1 μs, both the intensity and the complexity of the concentric-ring pattern evolve.

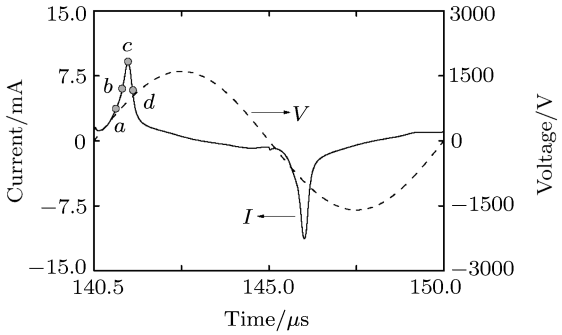


Fig. 1. The global current in positive half-cycle. The spots a, b, c and d correspond to the time scales 140.6 μs, 140.8 μs, 141.0 μs and 141.1 μs respectively.

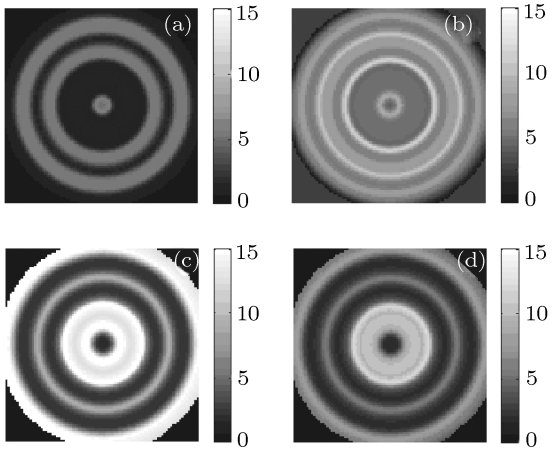


Fig. 2. The total current density at 140.6 μs (a), 140.8 μs (b), 141.0 μs (c), 141.1 μs (d) with the unit of mA/cm^2.

In Fig. 2(a), the discharge is characterized by two rings and a central spot. This evolves into a pattern of four bright concentric-rings that decay over a spatial scale of 1–2 mm in Fig. 2(b). At $t = 141.0$ μs when the discharge current reaches its positive peak, the pattern is now dominated by a very bright and broad ring close to the centre and an equally bright ring at the electrode edge sandwiching a less bright narrow ring located at a radius of $r = 4$ mm as shown in Fig. 2(c). As the discharge current reduces from its peak, the concentric-ring pattern changes little apart from reduced current density as shown in Fig. 2(d).

Figure 3 shows the 2D profile of the electron density at the axial position for the maximum electron density and again at the four instants of 140.6, 140.8, 141.0 and 141.1 μs. Again these show a clear pattern of concentric rings. As shown in Fig. 3(a), the electron avalanches are first triggered at the locations with the radii of 0.15 mm, 3.3 mm and 4.95 mm. Subsequently at 140.8 μs and in Fig. 3(b), this first set of discharge rings is extinguished and the electron avalanches are triggered at three other locations of $r = 1.05 - 2.55$ mm, 4.05 mm and 5.85 mm. In Fig. 3(c), the electron density at $r = 5.85$ mm is stronger than that at $r = 4.05$ mm, possibly due to the different charge accumulation and the nonlinear charge transport. The corresponding maximum electron densities are 4.2×10^{11} cm^{-3} and 2.2×10^{11} cm^{-3} respectively. It is clear that the electron density at the peak discharge current in Fig. 3(c) is several times greater than that in Fig. 3(a), which is about half-way towards the current peak. Finally at 141.1 μs and in Fig. 3(d), the electron density becomes smaller.

In DBD, nonlinearities in the charge transport in the background gas and the boundary conditions on the dielectrically insulated electrodes are critical in determining the appearance of complex spatiotemporal discharge structures.[8,23] During the first half-cycle, the pattern of the two rings and a central spot discharge at 140.6 μs is seen to be caused by three avalanches at $r = 0.15$, 3.3 and 4.95 mm. This is consistent with Fig. 4 in which the surface charge density on the dielectric barrier surface is plotted as a function of time for seven radial locations. At $t = 140.6$ μs, the surface charge density at $r = 0.15$, 3.3 and 4.95 mm has a large negative value which is resulted from the residual charges from the previous half cycle. This increases the gas voltage and enhances the electric field in the gas gap to trigger the three avalanches at $r = 0.15$, 3.3 and 4.95 mm. As shown in Fig. 5(a), the electric field can reach as large as 19 kV/cm at the momentary cathode at $z = 2.2$ mm. The locations at which the electric field reaches its local maximum are again at $r = 0.15$, 3.3 and 4.95 mm.

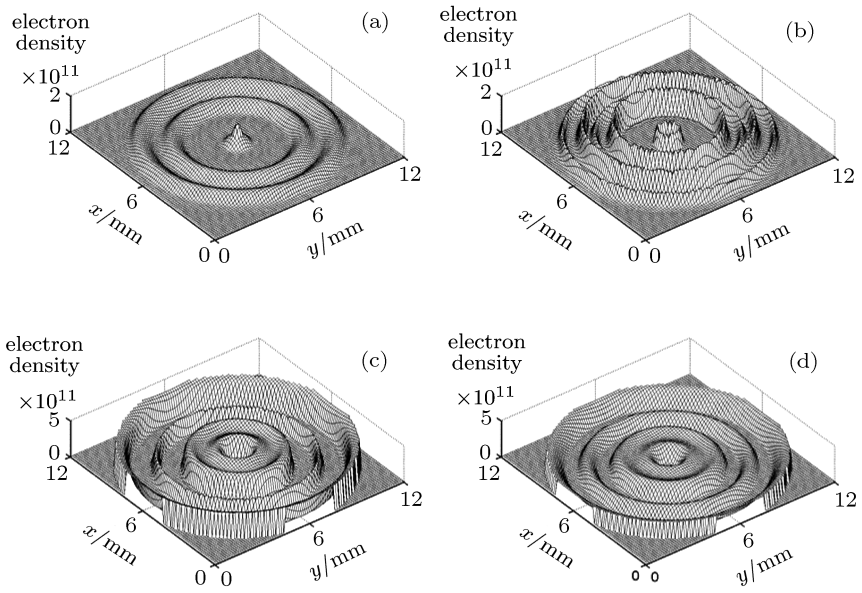


Fig. 3. The spatial-temporal evolution of electron density at 140.6 μs (a), 140.8 μs (b), 141.0 μs (c), and 141.1 μs (d).

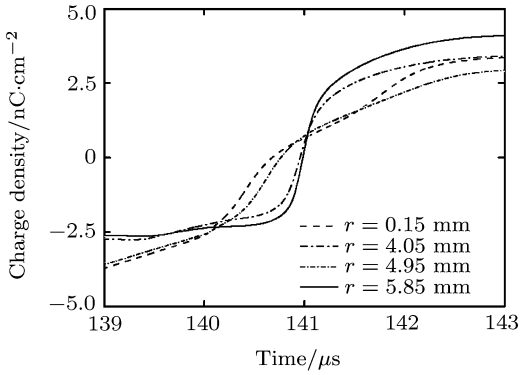


Fig. 4. The charging process on the barrier surface in positive half-cycle.

As the discharge current reaches its maximum at $t = 141.0$ μs, the surface charge density is seen in Fig. 4 to have a narrow distribution and the electric field in Fig. 5(b) is seen to have two large peaks, at $r = 1.05 - 2.55$ mm and $r = 5.85$ mm, sandwiching a smaller peak at $r = 4.05$ mm. These are consistent with the spatial profile of the current density in Fig. 2(c) and the electron density in Fig. 3(c). It is worth mentioning that the peak electric field in Fig. 5(b) is 28 kV/cm. Spatial distributions of the current density, the electron density and the electric field evolve as a result of gas breakdown and electron avalanches triggered by the axial electric field as well as the radial charge diffusion. It should be pointed out that the deposited charges at $r = 3.3$, 1.05 and 2.55 mm are not shown in Fig. 4 for the definition of the picture.

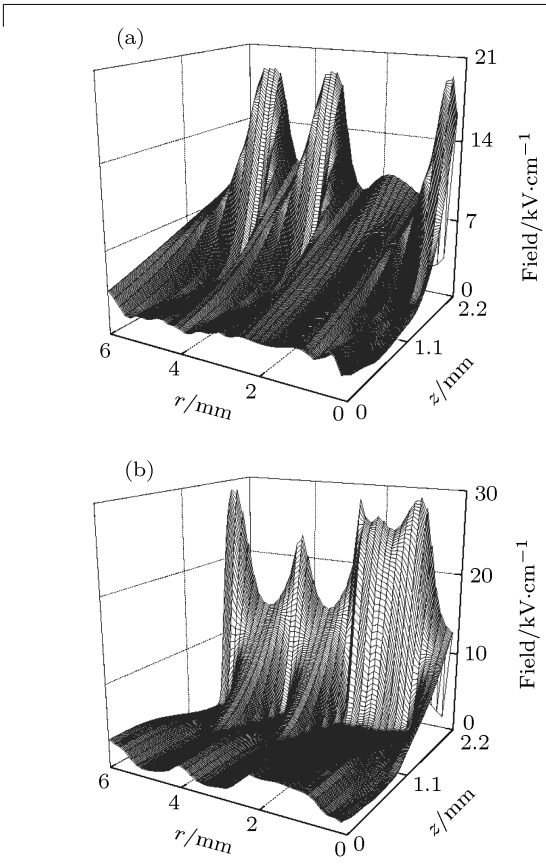


Fig. 5. Spatial variations of the electric field at 140.6 μs (a) and 141.0 μs (b).

The formation and development of the concentric-ring discharge structures have been explained above from the viewpoint of electron avalanches. They can also be understood from the evolution of individual

discharge rings.[27,28] The radial and axial shapes of the electron density in our azimuthally symmetrical model are shown in Fig. 6 where the momentary cathode is at $z = 2.2$ mm. In Fig. 6(a), three rings marked as 1, 2 and 3 are seen at $r = 0.15$, 3.3 and 4.95 mm respectively. After 0.2 s at $t = 140.8$ μs, ring 2 has split up into two rings marked as 2-a and 2-b whereas ring 3 has also split into two other rings marked as 3-a and 3-b as shown in Fig. 6(b). At $t = 140.9$ μs in Fig. 6(c), ring 1 turns into two parts with the one marked as 1-b moving towards ring 2-a. Simultaneously, ring 2-b and ring 3-a move towards each other and combine together as a new ring marked 4. Ring 3-b moves further towards the edge of the electrode where there was previously no gas breakdown. The distance between the 1-b and 2-a rings is now smaller. As time evolves further to $t = 141.0$ μs, ring 1-b and ring 2-a merge to form a new ring as marked 5. Ring 4 and ring 3-b do not appear to have moved radially but their electron density has undergone clear changes. It is worth mentioning that the ring structure appears to be strongest near the momentary cathode and possibly near the boundary between the sheath and the plasma bulk.[29]

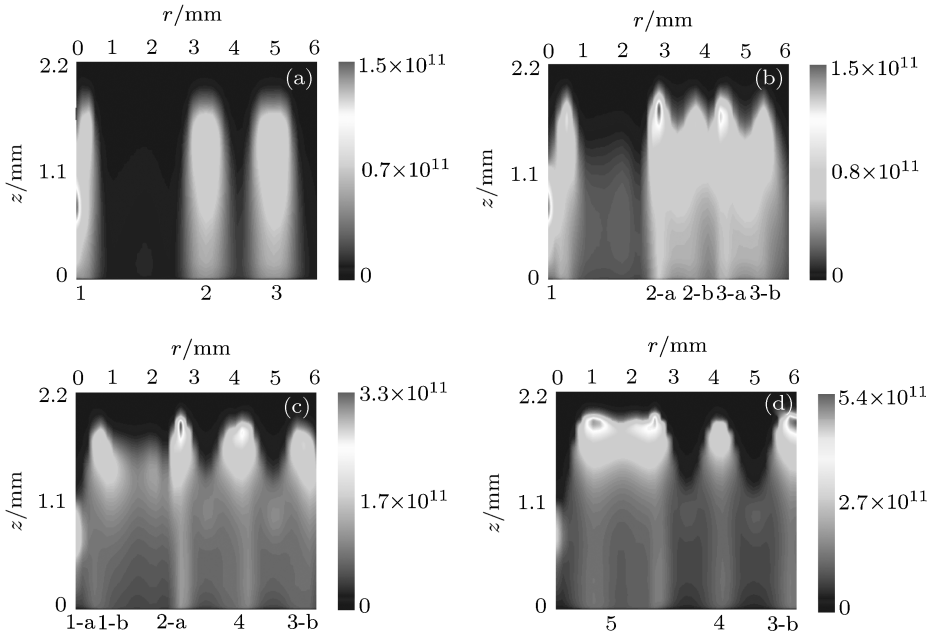


Fig. 6. The time evolution of the electron density in the negative half-cycle. The figures (a), (b), (c) and (d) correspond to 140.6 μs, 140.8 μs, 140.9 μs, 141.0 μs. The moment cathode is at the top side.

4. Conclusion

In this paper, a self consistent 2D fluid model was used to investigate the spatiotemporal evolution of an atmospheric helium DBD. A concentric-ring discharge structure has been demonstrated and its evolution has been shown to be characterized by an alternative occurrence of electron avalanches and discharge extinction in the radial direction. Surface charges on the dielectrically insulated electrodes and charge diffusion in the radial direction are important. Finally it has been shown that the concentric-ring structure appears near the momentary cathode and the atmospheric DBD structure near the anode is predominately uniform.

References

[1] Kogelschatz U 2002 *IEEE Trans. Plasma Sci.* **30** 1400
[2] Liang Z, Lü B, Luo H Y and Wang X X 2009 *Chin. Phys.* B **18** 646
[3] Dong L F, Fan W L, He Y F and Xiao H 2009 *Acta Phys. Sin.* **58** 94 (in Chinese)
[4] Gurevich E L, Zanin A L, Moskalenko A S and Purwins H G 2003 *Phys. Rev. Lett.* **91** 154501
[5] Gollub J P and Langer J S 1999 *Rev. Mod. Phys.* **71** S396
[6] Ristow G H 1995 *Pattern Formation in Granular Materials* (Berlin: Springer)
[7] Thompson K L, Bajaj K L S and Ahlers G 2002 *Phys. Rev.* E **65** 046218

[8] Maini P K, Painter K J and Chau H N P 1997 *J. Chem. Soc. Faraday Trans.* **93** 3601
[9] Dong L F, Liu F C, Liu S H, He Y F and Fan W L 2005 *Phys. Rev.* E **72** 046215
[10] Radu I, Bartnikas R and Wertheimer M R 2005 *IEEE Trans. Plasma Sci.* **33** 280
[11] Shirafuji T, Kitagawa T, Wakai T and Tachibana K 2003 *Appl. Phys. Lett.* **83** 2309
[12] Brauer I, Bode M, Ammelt E and Purwins H G 2000 *Phys. Rev. Lett.* **84** 4104
[13] Pismen L M 2001 *Phys. Rev. Lett.* **86** 548
[14] Yang Y, Shi J J, Harry J E, Proctor J, Garner C P and Kong M G 2005 *IEEE Trans. Plasma Sci.* **33** 298
[15] Guikema J, Miller N, Niehof J, Klein M and Walhout M 2000 *Phys. Rev. Lett.* **85** 3817
[16] Wang Y H, Zhang Y T, Wang D Z and Kong M G 2007 *Appl. Phys. Lett.* **90** 071501
[17] Deng X T, Shi J J, Shama G and Kong M G 2005 *Appl. Phys. Lett.* **87** 153901
[18] Brauer I, Punset C, Purwins H G and Boeuf J P 1999 *J. Appl. Phys.* **85** 7569
[19] Steinle G, Neundorf D, Hiller W and Pietralla M 1999 *J. Appl.* D **32** 1350
[20] Radehaus C, Dohmen R, Willebrand H and Niedernostheide F 1990 *J. Phys. Rev.* A **42** 7426
[21] Zhang P and Kortshagen U 2006 *J. Phys.* D **39** 153
[22] Zhang Y T and Wang D Z 2005 *J. Appl. Phys.* **98** 113308
[23] Stollenwerk L 2006 *Phys. Rev. Lett.* **96** 255001
[24] Kulikovsky A A 1994 *J. Phys.* D **27** 2556
[25] Kulikovsky A A 1994 *J. Phys.* D **27** 2564
[26] Ward A L 1962 *J. Appl. Phys.* **33** 2789
[27] Raizer Y P 1991 *Gas Discharge Physics* (New York: Springer)
[28] Zhang Y T, Wang D Z and Wang Y H 2005 *Phys. Plasmas* **12** 103508
[29] Shi J J and Kong M G 2003 *J. Appl. Phys.* **94** 5504